The H + N2O → OH + N2 Reaction Dynamics on an Interpolated QCISD Potential Energy Surface. A Quasiclassical Trajectory Study

ARTICLE *in* THE JOURNAL OF PHYSICAL CHEMISTRY A · JULY 2004

Impact Factor: 2.69 · DOI: 10.1021/jp048366b

3 AUTHORS, INCLUDING:

Jesus F Castillo
Complutense University of Madrid
76 PUBLICATIONS **2,058** CITATIONS

ARTICLES

The H + N_2O → OH + N_2 Reaction Dynamics on an Interpolated QCISD Potential Energy Surface. A Quasiclassical Trajectory Study

J. F. Castillo,* F. J. Aoiz, and L. Bañares

Departamento de Química Física I, Facultad de Química, Universidad Complutense, 28040 Madrid, Spain

M. A. Collins

Research School of Chemistry, Australian National University, Canberra, ACT

Received: April 14, 2004; In Final Form: June 2, 2004

A global ab initio interpolated potential-energy surface (PES) for the H + N_2O → OH + N_2 reaction has been constructed using the GROW package of Collins and co-workers. The ab initio calculations have been performed using the quadratic configuration interaction with single and double excitations (QCISD) and QCISD with quasipertubative treatment of triple excitations QCISD(T) methods. By use of this PES, a detailed quasiclassical trajectory study of integral and differential cross sections, product rovibrational populations and internal energy distributions are presented. It is found that the main mechanism for the title reaction is via an indirect process in which the H atom attaches to the N end of N_2O and then undergoes a 1,3-hydrogen shift, leading to products. However, the direct abstraction process in which the H atom attacks the O end generating OH + N_2 products accounts for ∼30% of the global reactivity at 1.5 eV collision energy. Both mechanisms contribute distinctly to the various reaction properties, and it is demonstrated that the trajectories associated with the direct mechanism have shorter collision times than those proceeding via the indirect mechanism. The theoretical integral cross sections as a function of collision energy are in good agreement with the experimental values at translational energies below 1.20 eV. At higher collision energies, the theoretical calculations on the present PES predict values of the cross sections smaller than those determined experimentally. The OH vibrational branching ratio OH($v' = 1$)/OH($v' = 0$) given by the theoretical calculations is considerably larger than that obtained experimentally by Brouard and co-workers. However, the calculated OH($v' = 0,1$) rotational populations at 1.48 eV reproduce to a large extent the measurements. Also, a good accordance is found with the experimental OH state resolved differential cross sections at 1.48 eV. The calculated kinetic energy release distributions and triple scattering angle-recoil velocity differential cross sections for state-resolved OH(v',N') products show that a substantial fraction of the total energy goes into rotational excitation of the N_2 coproduct due to the direct mechanism and that there exists a strong pair correlation in the angular and velocity distributions of the product molecules formed in coincidence.

I. Introduction

The reaction

$$H(^2S) + N_2O(^1\Sigma) \rightarrow OH(\tilde{X}^2\Pi) + N_2(^1\Sigma_g^+) \qquad \Delta_r H_o^\ominus = -2.706 \text{ eV} \quad (1)$$

has been studied extensively both experimentally and theoretically. For a recent review, see ref 1. In the pioneering photon-initiated experiments carried out by Hollingsworth et al.[2] and Wittig and co-workers,[3−5] the OH(X), OH(Ã), and NH(X) branching ratios, OH product quantum state populations, and kinetic energy release fractions of the H + N_2O → OH + N_2 and H + N_2O → NH + NO reactions were determined. In particular, OH Doppler-resolved laser-induced fluorescence (LIF) measurements,[5] using photolysis of HI as the H atom precursor, revealed that the N_2 product molecules are formed with a large internal excitation that was attributed to vibrationally excited N_2 molecules produced by a reaction mechanism in which a HNNO complex is formed and subsequently undergoes a 1,3-hydrogen shift to the N_2−OH product channel.

From the theoretical point of view, the first study of the stationary points of the HN_2O potential-energy surface (PES) was carried out by Marshall et al.[6] using the bond additive corrections Möller−Plesset 4 (BAC-MP4) methodology. According to this study, the reaction can presumably proceed either via a *direct* process, in which the H attacks the O end of N_2O, or via an *indirect* process, in which the H attaches to the terminal N to form a HNNO complex, followed by a 1,3-hydrogen migration yielding N_2 + OH. This early ab initio calculation[6] predicted a N−N bond length of 1.23 Å for the *cis*-HNNO intermediate, which is about 0.13 Å larger than the N_2

* To whom correspondence may be addressed. E-mail: jfc@legendre.quim.ucm.es.

10.1021/jp048366b CCC: $27.50
Published on Web 07/20/2004

TABLE 1: Energies of the Stationary Points of the H + N_2O $^2A'$ PES Including the Zero-Point Energy Correction[a]

species	QCISD/cc-pVDZ	QCISD(T)/cc-pVDZ	QCISD/cc-pVTZ	QCISD/cc-pVTZ[b]	QCISD(T)/cc-pVTZ[c]
H−ONN	0.91	0.91	0.86	0.86	0.84
H−NNO	0.54	0.55	0.51	0.50	0.49
[NNOH]	0.83	0.78	0.72	0.72	0.72
cis-HNNO	−0.58	−0.48	−0.66	−0.67	−0.59
trans-HNNO	−0.76	−0.69	−0.88	−0.88	−0.84
OH+N_2	−2.94	−2.35	−3.03	−3.03	−2.73
NH + NO	0.90	1.22	1.04	1.04	1.38

[a] All energies are in eV relative to H + N_2O. [b] The QCISD/cc-pVTZ calculation using the optimized QCISD/cc-pVDZ geometries. [c] The QCISD(T)/cc-pVTZ calculation using the optimized QCISD/cc-pVDZ geometries.

equilibrium distance, suggesting the formation of vibrationally excited N_2 products, as proposed by Wittig and co-workers.[5] A more complete characterization of the HN_2O PES was performed by Walch[7] using high-level ab initio methods, i.e., the complete active space self-consistent field/internally contracted configuration interaction (CASSCF/ICCI) method. Walch's calculations showed that the *indirect* pathway has a lower overall barrier and should be the more likely process at low collision energies.

The dynamics of the H + N_2O and its reverse NH + NO reactions were studied using the quasiclassical trajectory (QCT) method by Bradley et al.[8,9] on a global PES (hereafter, BS PES), based on the ab initio calculations of Walch[7] and on additional, less accurate, ab initio data obtained to better describe the reaction path for the 1,3-hydrogen migration and for the H addition to N_2O via the H−ONN transition state.[8] The energetics of the stationary points of the BS PES was modified with respect to the original calculations of Walch by fixing the difference between NH + NO and H + N_2O at the experimental exoergicity.[8] The QCT study of the H + N_2O reaction on that PES by Bradley and Schatz[9] showed that the *direct* mechanism for production of OH + N_2 was dominant for collision energies above 0.8 eV. However, these calculations predicted that OH and N_2 products were born with low rotational and vibrational excitation, with most of the available energy going into translation, at variance with the experimental observations of Böhmer et al.[5]

In a recent work, Fletcher and Wocjick[10] have measured the total reaction cross section as a function of collision energy, $\sigma_R(E_t)$, for the title reaction in a bulk experiment over collision energies in the range 0.87−1.95 eV. OH product molecules were detected by LIF, and several different H-atom precursors were used to span that range of collision energies. Absolute values of $\sigma_R(E_t)$ were estimated by calibration using the photodissociation of HNO_3 at 266 nm as an internal standard, for which the absorption cross section and quantum yield for the production of OH are very well known. The $\sigma_R(E_t)$ values were found to be about four times smaller that those calculated by Bradley and Schatz.[9] This large discrepancy between QCT and experiment was attributed to inaccuracies of the BS PES.

The most complete experimental studies for the title reaction have been carried out by Brouard and co-workers using a pump−probe experiment with sub-Doppler resolution at a mean collision energy of 1.48 eV.[11−14] In these experiments, OH rovibrational quantum-state populations, state-resolved differential cross sections (DCS), and the OH rotational angular momentum polarization were measured. In addition, information about the internal energy distribution of the undetected N_2 partner was obtained from the analysis of the kinetic energy release distributions for selected quantum states of the detected OH product molecules. In particular, kinetic energy distributions for selected rovibrational OH states showed a clear bimodal character, correlating with low and high internal excitation of the N_2 products. This behavior was interpreted in terms of two mechanisms: one yielding products with a high kinetic energy release (cold N_2 coproduct), presumably *direct*, and another that generates N_2 molecules with high internal excitation, attributed to an *indirect* process. The similarities found in the energy disposal for the photodissociation of N_2O in its first absorption band and that corresponding to the latter mechanism of the reaction lead the authors to suggest that N_2 generated via reaction 1 was born highly rotationally, rather than vibrationally excited.

In a previous work, Castillo et al. carried out a QCT study of the title reaction employing an interpolated ab initio PES.[1] The PES was developed using the iterative interpolation methods devised by Collins and co-workers[15−19] and recently implemented in the GROW package. The Becke three-parameter nonlocal exchange functional[20] with the nonlocal correlation of Lee, Yang, and Parr (B3LYP) hybrid density functional theory (DFT) was used for the ab initio calculations. QCT calculations on this PES predicted the existence of two pathways, as anticipated by Brouard and co-workers, one associated with the attack of the H to the O end of the N_2O molecule, and a second one in which the initial configuration corresponds to H−NNO, followed by the formation of the *cis*-HNNO, which, after the migration of the H, would give rise to OH formation. This latter mechanism would be *indirect*, whereas the former would be more *direct*. It was found that the direct mechanism on that PES constituted the main process for the reaction and accounted for a considerable amount of internal excitation of N_2. The resulting N_2 vibrational distribution was *cold*, while the rotational distribution was quite *hot*. In contrast, the indirect mechanism yielded a relatively cold rotational distribution, thus explaining the bimodality of the recoil energy distributions of the N_2 coproduct associated with the formation of a particular rovibrational state of the OH product that was observed experimentally. Therefore, it is the direct mechanism that is responsible for the N_2 rotational excitation, in contrast with the interpretation of Brouard and co-workers, who conjectured that the indirect mechanism would yield rotationally excited N_2.

Nevertheless, some of the experimental results were not well reproduced by the QCT calculations on the B3LYP/cc-pVTZ PES.[1] In particular, the OH state-resolved differential cross sections were clearly at variance with those experimentally deduced. In addition, the DFT ab initio calculations predicted a H−ONN transition state at a lower energy than that of the [NNOH] intermediate, in disagreement with previous higher level ab initio electronic correlation calculations (CASSCF/ICCI),[7] which yielded a similar energy for the [NNOH] transition state, but a H−ONN transition state at a substantially higher energy (see Table 1 in ref 1). It is expected that some of the discrepancies found between theory and experiment may be diminished if a PES based on higher-level ab initio theory were constructed. In the present work, a QCT study of the title reaction at collision energies in the range E_t = 1.0−1.56 eV

TABLE 2: Energies of the Stationary Points of the H + N_2O PES Including the Zero-Point Energy Correction[a]

species	QCISD(T) cc-pVTZ	CCSD(T)/CBS{Q,5}[b]	CASSCF/ICCI/cc-pVTZ[c]	G3X[d]	G2[e]	B3LYP/cc-pVTZ[f]
H−ONN	0.84		0.78		0.69	0.55
H−NNO	0.49	0.31	0.45	0.42	0.40	0.25
[NNOH]	0.72	0.75	0.71	0.83	0.81	0.71
cis-HNNO	−0.59	−0.75	−0.63	−0.51	−0.67	−0.88
trans-HNNO	−0.84	−1.00	−0.86	−0.90	−0.93	−1.16
OH+N_2	−2.73	−2.77		−2.72	−2.71	−2.56
NO + NH	1.38	1.54	1.37	1.48	1.50	1.47

[a] All energies are in eV relative to H + N_2O. [b] Reference 25. [c] Reference 7. [d] Reference 25. [e] This work. [f] Reference 1.

has been carried out on a new ab initio interpolated PES. The quadratic configuration interaction with single and double excitations (QCISD) and QCISD with quasipertubative treatment of triple excitations, QCISD(T), methods have been employed to explore and construct the PES. These methods appear to be better suited to treat transition states of open-shell species than the unrestricted Möller−Plesset many-body perturbation theory[21] due to the "spin-contamination" problem.

II. Potential Energy Surfaces

The ab initio calculations have been carried out using the Gaussian 98 suite of programs.[22] The energies and geometries of the relevant stationary points of the H + N_2O($^2A'$) PES have been calculated using QCISD and QCISD(T) in conjunction with the correlation-consistent basis sets cc-pVDZ and cc-pVTZ.[23] Table 1 shows the relative energies of the stationary points with respect to the H + N_2O asymptote and including zero-point energy corrections. The experimental exothermicity at 0 K for the H + N_2O → OH + N_2 reaction is $\Delta_r H_0^\circ = -2.71 \pm 0.04$ eV,[24] which compares very well with the QCISD(T)/cc-pVTZ result of −2.73 eV. For the H + N_2O → NH + NO reaction, the QCISD(T)/cc-pVTZ calculation slightly underestimates (8%) the experimental endothermicity $\Delta_r H_0^\circ = 1.50$ eV.[24]

Table 2 shows the comparison between the present QCISD-(T)/cc-pVTZ calculations and previous ab initio calculations, including new calculations at Gaussian-2 (G2) level of theory performed in this work. As can be seen, the agreement with the CASSCF/ICCI/cc-pVTZ energies by Walch[7] is remarkably good. However, the G2 and B3LYP/cc-pVTZ methods predict a barrier of the H−ONN transition state much lower than that of the [NNOH] saddle point, whereas QCISD(T)/cc-pVTZ and CASSCF/ICCI/cc-pVTZ yield the opposite. In addition, all the calculations indicate that the H−NNO transition-state energy is considerably lower than that of the H−ONN transition state. The *trans*-HNNO structure is found to be below the *cis*-HNNO minimum, in accordance with all previous calculations, except the BAC-MP4 prediction of Marshall and co-workers,[6] who found the reverse order. As it will be shown below, the differences found between the QCISD(T)/cc-pVTZ and B3LYP/cc-pVTZ calculations have important effects on the overall dynamics of the title reaction.

Tables 3−6 present the QCISD/cc-pVDZ- and QCISD/cc-pVTZ-computed frequencies and optimized geometries of the stationary points. It should be noted that all the transition states have a planar geometry. The reactant N_2O and products OH + N_2 bond lengths are in very good agreement with experimental determinations with a relative difference no larger than 0.9%. The N_2O, OH, and N_2 vibrational frequencies are about 1% within the experimental values. The comparison with the CASSCF (with a polarized double-ζ set of Dunning and Hay) calculations by Walch[7] is good in all cases. Recently, Laursen et al.[26] have investigated the NH + NO reaction in a solid Xe matrix and have detected the HNNO intermediate by IR spectroscopy. Two isomers were identified that were associated to *cis*-HNNO and *trans*-HNNO structures. The assigned experimental frequencies for these structures are in quite good agreement with the present QCISD results and with those obtained using CASSCF/ICCI by Walch[7] and Gaussian-2. It should be noticed that the geometries and frequencies calculated using the cc-pVDZ basis are quite similar to those obtained when the cc-pVTZ basis is employed. This indicates that the optimization of the geometries carried out using the smaller basis is of comparable accuracy with that obtained when using the larger basis.

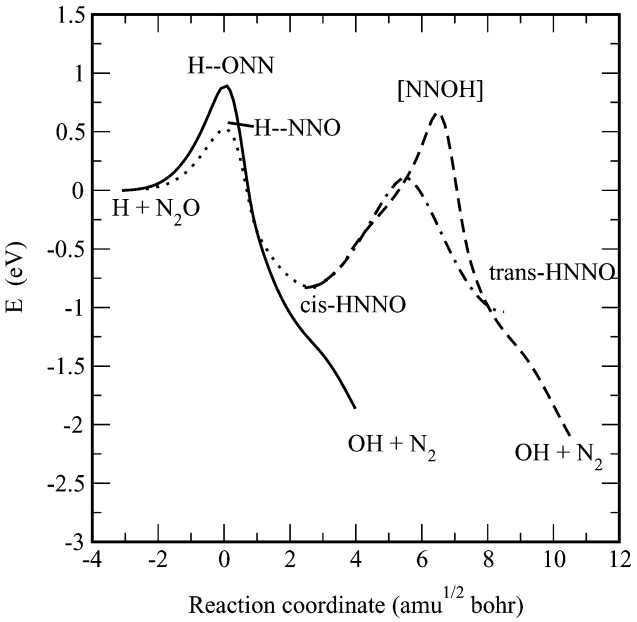

Figure 1. MEPs of the H + N_2O → OH + N_2 reaction computed at the QCISD/cc-pVDZ level of theory. Energies are relative to the H + N_2O asymptote (−184.712033 hartree). Solid line, MEP for the H + N_2O → H−ONN → OH + N_2 *direct* mechanism. Dotted line, MEP for the H + N_2O → H−NNO → *cis*-HNNO. Dashed line, MEP for the *cis*-HNNO → [HONN] → OH + N_2 migration. Dot−dashed line, MEP for the *cis*-HNNO → *trans*-HNNO isomerization.

From the H−NNO, H−ONN, and [NNOH] transition states and cis-to-trans isomerization, the intrinsic reaction coordinate (IRC) or minimum energy paths (MEP) have been calculated at the QCISD/cc-pVDZ level of theory using the Berny algorithm implemented in Gaussian 98.[22] The MEPs are displayed in Figure 1. As can be seen, the H−NNO transition state is connected to the *cis*-HNNO minimum, and the [NNOH] transition state connects the *cis*-HNNO to the OH + N_2 products. The set of points that define the reaction paths shown in Figure 1 have been used to calculate the initial surface. A total of 200 points for the reaction paths have been calculated and used as an initial guess for developing the PES. The self-consistent field (SCF) wave function has been required to be converged tight to 10^{-10} and to be stable for all points. The global PES has been grown using the iterative methods

implemented in the GROW script, using the QCISD/cc-pVDZ ab initio level of theory. The QCISD/cc-pVDZ level has been chosen to grow the PES because analytical gradients are available and second derivatives can be computed at a reasonable cost. The methods for choosing a new data point at each iteration have been discussed in detail elsewhere. The "variance sampling"[27] and "h weight" methods[28,29] have been used alternatively for each additional data point. The classical trajectory calculations, which are performed in order to select new data points, have been run under the following conditions. A ground-state zero-point energy has been given to N_2O with coordinates and momenta corresponding to a microcanonical distribution. A relative translational energy of 1.48 eV and a maximum impact parameter of 2.0 Å were chosen for the initial conditions of the trajectories. Both the initial and final relative separation of the H atom to the N_2O molecule and of the OH and N_2 products, respectively, was set to 6 Å. A total of 1100 data points that include energy and first and second derivatives have been calculated for the present PES. The convergence of the total integral cross section has been monitored, while the surface was being developed by running batches of 2000 trajectories. The cross section only changes by less than 0.5% when the number of ab initio points is increased from 1000 to 1100. As we noted above, it is necessary to use the QCISD-(T)/cc-pVTZ level of theory to reproduce the experimental entalpies at 0 K for the OH + N_2 and NH + NO reactions. Thus, we have replaced the energies of the 1100 points that define the present PES by those calculated using the QCISD-(T)/cc-pVTZ level of theory. The great advantage of employing the GROW package is the need of a relatively small number of ab initio points to carry out the dynamical calculations accurately without the need of performing any fit to a global analytical form of the PES.

III. Quasiclassical Trajectory Calculations

The methodology used in the QCT calculations is essentially the same as that described in the recent studies on the H + H_2O[30−32] and H + N_2O[1] reactions. Batches of 5×10^4 trajectories with a maximum impact parameter $b_{max} = 2.10$ Å have been run for each translational energy in the range $E_t = 0.6-1.48$ eV. At $E_t = 1.48$ eV, an additional batch of 4.3×10^5 trajectories was run to improve the product state-resolved statistics. Initial conditions for the rotationless N_2O molecule in the (000) vibrational state have been determined using a fixed microcanonical normal mode sampling. Integration of the equations of motion was carried out using an adapted version of the VENUS96 program[33] with a time step of 0.05 fs. The typical conservation of energy was better than 1 in 10^5. The assignment of diatomic products quantum numbers has been carried out as in previous works, calculating the rovibrational levels of OH and N_2 by the semiclassical quantization of the classical action using in each case the asymptotic diatomic potentials of the PES. The classical rotational angular momenta are equated to $[j'(j'+1)]^{1/2}\hbar$. With the (real) j' value so obtained, the vibrational quantum number v' is found by equating the internal energy of the outgoing molecule to the corresponding rovibrational Dunham expansion in $(v' + {}^1/_2)$ and $j'(j'+1)$, whose coefficients are calculated by fitting the semiclassical rovibrational energies. The values of v' and j' found in this way are then rounded to the nearest integer.

To avoid inconsistencies due to a wrong conservation of total energy when the vibrational and rotational quantum numbers are equated to their nearest integers, the kinetic energy release, E_t', and the fractions of the total energy going into translation, vibration, or rotation are calculated quasiclassically by the following method. The available energy for the products (maximum translational energy consistent with the products' zero-point energy) is given by

$$E_{av} = E_t + \Delta D_e + E_{N_2O}(\{v_i\}, j) - E_{N_2}(v_{N_2} = 0, j_{N_2} = 0) - E_{OH}(v_{OH} = 0, j_{OH} = 0) = E_t + \Delta D_0 + [E_{N_2O}(\{v_i\}, j) - E_{N_2O}(\{v_i = 0\}, j = 0)] \quad (2)$$

where E_{N_2O}, E_{N_2}, and E_{OH} are the respective N_2O, N_2, and OH internal energies calculated from the minimum of the asymptotic potentials. ΔD_e and ΔD_0 are the differences of dissociation energies calculated from the minimum of the potentials of products and reagents and from their zero points, respectively. The term within brackets of the second line of eq 2 thus represents the N_2O internal energy above the zero-point energy. By use of the integer values determined for the vibrational and rotational quantum numbers for each trajectory, the product relative translational energy for each trajectory is given by

$$E_t' = E_t + \Delta D_e + E_{N_2O}(\{v_i\}, j) - E_{N_2}(v_{N_2}, j_{N_2}) - E_{OH}(v_{OH}, j_{OH}) = E_{av} - E_{N_2}(v_{N_2}, j_{N_2}) + E_{N_2}(v_{N_2} = 0, j_{N_2} = 0) - E_{OH}(v_{OH}, j_{OH}) + E_{OH}(v_{OH} = 0, j_{OH} = 0) \quad (3)$$

The fraction of the available energy channelled into translation, f_t, can be written as

$$f_t = \frac{E_t'}{E_{av}} = 1 - \frac{E_{OH}(v_{OH}, j_{OH}) - E_{OH}(v_{OH} = 0, j_{OH} = 0)}{E_{av}} - \frac{E_{N_2}(v_{N_2}, j_{N_2}) - E_{N_2}(v_{N_2} = 0, j_{N_2} = 0)}{E_{av}} \quad (4)$$

and the fractions into vibration, $f_{v,OH}$, and rotation, $f_{r,OH}$, for the OH product are given by

$$f_{v,OH} = \frac{E_{OH}(v_{OH}, j_{OH}) - E_{OH}(v_{OH} = 0, j_{OH})}{E_{av}} \quad (5)$$

$$f_{r,OH} = \frac{E_{OH}(v_{OH}, j_{OH}) - E_{OH}(v_{OH}, j_{OH} = 0)}{E_{av}} \quad (6)$$

with similar expressions for the N_2 molecule. It is easy to show that $f_t + f_{v,OH} + f_{r,OH} + f_{v,N_2} + f_{r,N_2} = 1$.

The f_t value calculated with eq 4 for each trajectory is used to obtain the distribution $P(f_t)$ by fitting the data to an expansion in Legendre polynomials. Similarly, the center-of-mass recoil velocity distribution of one of the products, e.g., $P(w_{OH})$, can be expressed as

$$P(w_{OH}) = \frac{2}{w_{max}} P(r) = \frac{2}{w_{max}} \sum_{m=0}^{M} b_m P_m(r) \quad (7)$$

where $r = 2f_t^{1/2} - 1$, $w_{max} = [2E_t' m_{N_2}/(m_{OH}\mathscr{M})]^{1/2}$ and $\mathscr{M} = m_{N_2} + m_{OH}$. The coefficients of the expansion of eq 7 are given by

$$b_m = \frac{2m+1}{2} \langle P_m(r) \rangle \quad (8)$$

where the average is performed over all the reactive trajectories.

When one of the products, for instance OH, is detected in a particular v, j state, it is convenient to define the fraction of

translational energy referred to a particular quantum state of this product. The available energy for the coproduct, N_2, in coincidence with the appearance of OH(v_{OH}, j_{OH}), $E_{av}(v_{OH}, j_{OH})$, can be written as

$$E_{av}(v_{OH}, j_{OH}) = E_t + \Delta D_e + E_{N_2O}(\{v_i\}, j) - E_{N_2}(v_{N_2} = 0, j_{N_2} = 0) - E_{OH}(v_{OH}, j_{OH}) = E_t + \Delta D_0 + [E_{N_2O}(\{v_i\}, j) - E_{N_2O}(\{v_i = 0\}, j = 0)] - E_{OH}(v_{OH}, j_{OH}) + E_{OH}(v_{OH} = 0, j_{OH} = 0) \quad (9)$$

The translational relative energy for the formation of N_2 in a v_{N_2}, j_{N_2} state will be thus given by

$$E_t'(v_{N_2}, j_{N_2}|v_{OH}, j_{OH}) = E_{av}(v_{OH}, j_{OH}) - E_{N_2}(v_{N_2}, j_{N_2}) + E_{N_2}(v_{N_2} = 0, j_{N_2} = 0) \quad (10)$$

whereas the fraction of the available energy going into translation for a *fixed* internal state of the OH molecule can be defined as

$$\tilde{f}_t = \frac{E_t'(v_{N_2}, j_{N_2}|\, v_{OH}, j_{OH})}{E_{av}(v_{OH}, j_{OH})} \quad (11)$$

The calculation of the distribution $P(\tilde{f}_t)$ has been carried out by using the state-resolved integral cross sections as described in recent works.[31,32]

To calculate the differential cross sections (DCS), the scattering angle in the center-of-mass (CM) frame has been defined as that formed between the incoming H atom and the outgoing OH radical. This is consistent with the convention of the experiments of Brouard and co-workers,[11−14] in which the OH is the product molecule detected. Thus, the definition of the scattering angle θ is given by

$$\cos\theta = \frac{\mathbf{w}_H \cdot \mathbf{w}_{OH}}{|\mathbf{w}_H||\mathbf{w}_{OH}|}, \quad (12)$$

where $\mathbf{w}_{OH}$ and $\mathbf{w}_H$ are the OH and H atom CM velocities, respectively.

The DCSs are calculated by the method of moments expansion in Legendre polynomials. The Smirnov−Kolmogorov test is used to decide when to truncate the series. Significance levels higher that 95% can be achieved using 3−4 moments, ensuring good convergence, such that the inclusion of more terms does not produce significant change.

Polar maps representing the triple-scattering angle-recoil velocity are calculated by fitting the QCT results to an expansion in a double series of Legendre polynomials of the form

$$\frac{d^3\sigma_R}{d\omega\, dw_{OH}} = \frac{2}{w_{max}^2}\frac{\sigma_R}{2\pi}\sum_n^N\sum_m^M \alpha_{nm}P_n(\tilde{r})P_m(\cos\theta) \quad (13)$$

where w_{max} is the maximum CM recoil velocity for a given rovibrational state of the OH molecule and $\tilde{r} = 2\tilde{f}_t^{1/2} - 1$ with $\tilde{f}_t$ calculated using eq 11. The α_{nm} coefficients are calculated by Monte Carlo averaging over the number of reactive trajectories yielding a given v', j' state of the OH product

$$\alpha_{nm} = \frac{(2n+1)(2m+1)}{4}\langle P_n(\tilde{r})P_m(\cos\theta)\rangle \quad (14)$$

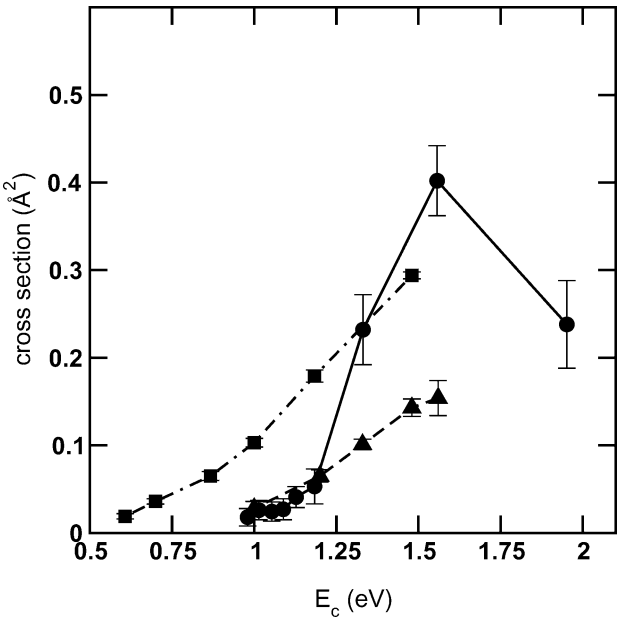

Figure 2. Total reaction cross section (in Å^2) as a function of collision energy (in eV) for the H + N_2O → OH + N_2 reaction. Solid triangles and dashed line, present QCT results. Solid circles and solid line, experimental results from ref 10. Solid squares and dot−dashed line, QCT results from ref 1.

Given the relatively small number of reactive trajectories for a given v', j' state of the OH product, the number of coefficients N and M used in the fitting procedure were typically 3−4. Numerical integration of the results of eq 13 over the scattering angle rendered $P(w_{OH})$ in excellent agreement with those calculated using eq 7 or the state-to-state integral cross sections.[31]

The collision time, τ_{col}, of every trajectory has been calculated as in previous works,[34,35] as $\tau_{col} = \tau_{tot} - \tau_i - \tau_f$, where τ_{tot} is the total time of the trajectory, τ_i is the time spent by the reagents as they approach before the interaction takes places, and τ_f is the time spent by the products to separate once the strong interaction has ceased. The values of τ_i and τ_f can be determined by defining previously initial and final relative distances, ρ_i and ρ_f, for which, on average, the strong chemical interaction occurs. In the present case, values of $\rho_i = \rho_f = 2$ Å have been employed.

IV. Results and Discussion

A. Total Reaction Cross Sections and Average Energy Disposals. The present QCT total reaction cross section as a function of collision energy, $\sigma_R(E_t)$, for the title reaction is shown in Figure 2. The present results agree quite well with the absolute values measured by Fletcher and Wocjick[10] at E_t < 1.2 eV. However, the experimental σ_R shows an abrupt increase for collision energies above 1.2 eV, while the present QCT results rise smoothly, and consequently the theoretical cross sections are considerably smaller than the experimental values at higher energies. The previous QCT σ_R calculations on the B3LYP/cc-pVTZ PES[1] predicted a significantly lower threshold for reaction and larger cross sections than the present ones at all the collision energies studied. The smaller cross sections obtained on the present PES in comparison with those calculated on the B3LYP/cc-pVTZ PES can be related to the smaller barriers of the H−NNO and H−ONN transition states in the latter (see Table 2). It is difficult to account for the differences in the absolute magnitude of the experimental and theoretical cross sections values. The former are subject to a considerable uncertainty since they imply a separate calibration

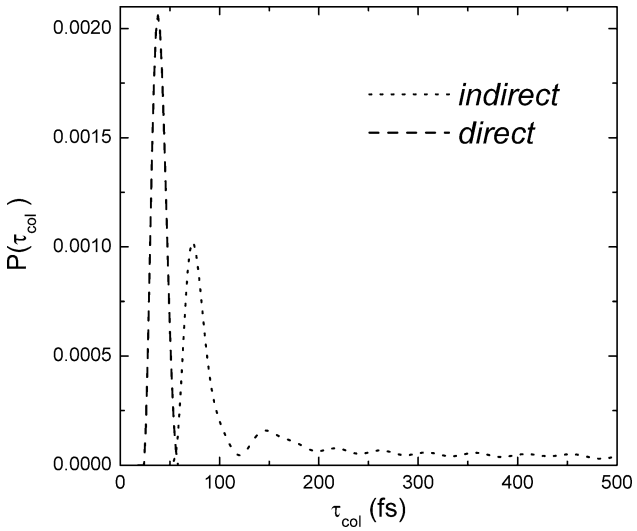

Figure 3. Distribution of collision times calculated at $E_t = 1.48$ eV on the present PES. Dotted line, contribution from *indirect* trajectories. Dashed line, contribution from *direct* trajectories. See text for details.

procedure based on the photolysis of HNO_3 at a fixed wavelength of 266 nm selecting a single quantum state of OH (the $R_1 5$ line), which is compared with the yield of the same line in the H + N_2O reaction producing the H atoms by photolysis of several precursors (HI and CH_3SH) at various wavelengths. This kind of calibration may lead to important errors in the absolute values of the cross section. As an instance of the possible errors in determining the absolute cross sections, recent experiments on the H + H_2O reaction have shown that a "in situ" calibration with the photolysis of water at the same wavelength determining the whole rotational distributions have yielded cross-section values almost an order of magnitude smaller than those previously reported, in much better agreement with theoretical (QCT and QM) predictions.[36] The calculated values on the previous B3LYP/cc-pVTZ PES[1] were about a factor of 2 larger than those obtained on the presumably more accurate present PES. In any case, assuming the experimental values as the correct ones, present calculations are closer to the these values than those given by the calculations of ref 9.

Considering the reaction paths presented in Figure 1, there are two possible mechanisms for the reaction: one in which the H atom attacks the O side of the N_2O molecule, forming H−ONN to yield products, and a second one, more complex, in which the H atom approaches first the terminal N atom, forming either the cis or trans H−N−N−O and, after overcoming a barrier, migrates to a [NNOH] structure, that finally decomposes into products. On simple grounds, one can expect the first mechanism, which is basically an abstraction, to be more direct than the second, which implies the formation of a complex and subsequent atom migration. The choice of one of these two mechanisms would be governed to a large extent by the direction of approach and the distance of the H atom to the N or O side of the molecule. Bradley and Schatz[9] proposed to label the reactive trajectories as *direct* or *indirect* according to which distance, O−H or N−H, first reaches a given small value. Considering the geometries of the stationary points shown in Tables 3−6, this value could be approximately established to be 1.6 Å. However, this classification has to be fully justified by inspection of the collision times, τ_{col}, of both mechanisms. Figure 3 shows the distribution of collision times, calculated as indicated in section III, for the reactive trajectories at 1.48 eV collision energy on the present PES. Essentially, this distribution consists of two well-differentiated peaks appearing

TABLE 3: Geometries and Vibrational Frequencies of the Stationary Poins of the H + N_2O PES Obtained Using QCISD/cc-pVDZ[a]

	H + N_2O	H−NNO	*cis*-HNNO	*trans*-HNNO	H−ONN
r_{NH}		1.549	1.043	1.031	
r_{NN}	1.138	1.161	1.241	1.254	1.150
r_{NO}	1.195	1.196	1.217	1.208	1.239
r_{OH}					1.437
∠HNN		111.0	107.6	105.5	
∠NNO	180.0	167.3	137.6	131.4	157.1
∠HON					113.0
ω_1	2345.1	2167.7	3284.5	3460.2	2137.7
ω_2	1312.2	1289.9	1722.9	1701.6	1195.5
ω_3	598.0	758.8	1346.7	1390.0	840.9
ω_4	598.0	389.1	1248.9	1292.4	472.8
ω_5		1405.0*i*	562.9	638.2	1946.2*i*
ω_6		619.5	810.0	824.0	570.6

[a] Distances (r) are in Å, angles in degrees, and frequencies (ω_i) in cm^{-1}.

TABLE 4: Geometries and Vibrational Frequencies of Stationary Points of the H + N_2O PES Obtained Using QCISD/cc-pVDZ[a]

	cis-to-*trans*-HNNO	[NNOH]	OH + N_2	NH + NO
r_{NH}	1.056	1.255		1.054
r_{NN}	1.231	1.227	1.114	
r_{NO}	1.209	1.434		1.166
r_{OH}	2.974	1.363	0.978	
∠HNN	112.8	89.2		
∠NNO	177.0	95.71		
∠NOH		77.0		
∠OHN		98.0		
ω_1	2982.4	2766.0	3726.8(OH)	3218.4(NH)
ω_2	1936.7	2087.9	2393.5(N_2)	1884.9(NO)
ω_3	1284.9	921.6		
ω_4	1159.2	649.7		
ω_5	906.7*i*	1859.9*i*		
ω_6	480.0	1021.7		

[a] Distances (r) are in Å, angles in degrees, and frequencies (ω_i) in cm^{-1}.

at collision times below 100 fs plus a long tail extending at larger collision times. The distribution of collision times corresponding to direct reactive trajectories (H−ONN) constitutes the first peak and is confined in a narrow range of collision times ($\tau_{col} \leq 60$ fs). The second peak and the remaining tail of the distribution is caused by the trajectories labeled as indirect (H−NNO). Therefore, the assignment according to the side of the molecule that is first attacked by the H atom indeed characterizes the actual duration of the reactive encounter very well. As can be seen in Figure 3, most of the reactive encounters do not last more than 200 fs, but since the tail decreases very slowly as τ_{col} increases, there are collisions that might last ~1 ps, even at a collision energy as high as 1.48 eV. From the relative areas of the distribution of τ_{col} corresponding to the two types of trajectories, it is already evident that the preferred mechanism is that occurring via *indirect* trajectories.

Table 7 presents the σ_R, energy partitioning, and the fraction of trajectories going through the *direct* and *indirect* mechanisms at the collision energies studied. As in previous works,[1,32] the fractions for vibration and rotation have been obtained from the rovibrational energies calculated by rounding off the vibrational and rotational actions of the products as discussed in section III. Thus, $f_t = 1$ corresponds to the formation of N_2 and OH molecules in their ground rovibrational state. As can be seen, the amount of available energy going into translation of the products ranges between 72 and 63% as collision energy increases. The fractions into rotation and vibration of OH and that into vibration of N_2 are fairly constant with collision energy

TABLE 5: Geometries and Vibrational Frequencies of the Stationary Points of the H + N_2O PES Obtained with QCISD/cc-pVTZ[a]

	H + N_2O	H−NNO	*cis*-HNNO	*trans*-HNNO	H−ONN
r_{NH}		1.547	1.030	1.018	
*r*NN	1.122	1.144	1.226	1.238	1.132
*r*NO	1.188	1.189	1.208	1.199	1.231
*r*OH					1.425
∠HNN		111.1	108.7	106.5	
∠NNO	180.0	168.4	138.4	132.2	158.6
∠HON					112.7
ω_1	2350.6	2182.6	3325.0	3497.2	2164.7
ω_2	1306.2	1286.3	1730.2	1710.9	1189.3
ω_3	622.2	764.0	1352.5	1392.0	843.4
ω_4	622.2	411.2	1249.2	1297.3	469.2
ω_5		1381.0*i*	576.7	650.4	1942.9*i*
ω_6		639.8	808.3	826.4	583.0

[a] Distances (*r*) are in Å, angles in degrees, and frequencies (ω_i) in cm^{-1}.

TABLE 6: Geometries and Vibrational Frequencies of Stationary Points of the H + N_2O PES Obtained with QCISD/cc-pVTZ[a]

	cis-to-*trans*-HNNO	[NNOH]	OH + N_2	NH + NO
r_{NH}	1.041	1.241		1.037
r_{NN}	1.217	1.206	1.098	
r_{NO}	1.201	1.434		1.153
r_{OH}	2.974	1.369	0.969	
∠HNN	111.2	90.2		
∠NNO	177.3	95.8		
∠NOH		76.4		
∠OHN		97.5		
ω_1	3055.8	2137.6	3772.4 (OH)	3292.1 (NH)
ω_2	1931.3	1688.0	2408.9 (N_2)	1811.4 (NO)
ω_3	1292.0	914.4		
ω_4	1166.6	645.1		
ω_5	920.8*i*	1997.9*i*		
ω_6	508.6	1023.8		

[a] Distances (*r*) are in Å, angles in degrees, and frequencies (ω_i) in cm^{-1}.

TABLE 7: QCT Total Reaction Cross Sections (σ_R) and Energy Partitioning Data for the H + N_2O Reaction at Different Collision Energies[a]

E_t/eV	σ_R/Å^2	$\langle f_t \rangle$	$\langle f_r^{OH} \rangle$	$\langle f_v^{OH} \rangle$	$\langle f_r^{N_2} \rangle$	$\langle f_v^{N_2} \rangle$	f_d	f_i
1.00	0.028	0.72	0.05	0.14	0.05	0.04	0.07	0.93
1.18	0.065	0.69	0.05	0.12	0.09	0.05	0.15	0.85
1.33	0.101	0.67	0.06	0.13	0.09	0.04	0.17	0.83
1.48	0.133	0.63	0.07	0.14	0.13	0.04	0.27	0.73
1.56	0.154	0.63	0.05	0.14	0.13	0.05	0.30	0.70

[a] f_d and f_i are the fractions of reactive trajectories going through the *direct* and *indirect* mechanisms, respectively (see text for details). Statistical uncertainties are ±0.003 Å^2 in the cross sections.

(about 13%, 5−6%, and 4−5%, respectively). However, the fraction into rotation of N_2 increases from 5% up to 13% at the expenses of the translational energy release.

The analysis of trajectories in terms of the collision times reveals that the *indirect* trajectories (H−NNO) are dominant at all energies and that the *direct* trajectories (H−ONN) become more important as collision energy increases. This is consistent with the fact that in the current PES *direct* trajectories have to overcome a barrier of 0.82 eV in the H−ONN transition state, while the barrier for the [NNOH] H-migration transition state is 0.72 eV. Thus, as collision energy increases and more energy is available to overcome the barriers, the direct mechanism becomes more important.

In contrast, the opposite distribution of direct and indirect trajectories was obtained in the QCT calculations on the B3LYP/cc-pVTZ PES at all the collision energies studied.[1] In that case, the indirect mechanism was gaining more importance as collision energy increased. This fact can be easily explained considering that in the B3LYP/cc-pVTZ PES the H−ONN barrier is 0.16 eV lower than the [NNOH] barrier. In addition, QCT calculations on the B3LYP/cc-pVTZ PES[1] predicted that a considerable amount of the available energy (about 25%) is transferred to N_2 rotation, at variance with the calculation on the present PES. Thus it does become evident that the direct trajectories are associated with the rotational excitation of the N_2 product.

TABLE 8: Energy Disposal Data for the H + N_2O Reaction at E_t = 1.48 eV[a]

$\langle f_t \rangle$	$\langle f_r^{OH} \rangle$	$\langle f_v^{OH} \rangle$	$\langle f_{int}^{N_2} \rangle$	$\langle f_r^{N_2} \rangle$	$\langle f_v^{N_2} \rangle$	
0.45 ± 0.04	0.06 ± 0.01	0.02 ± 0.01	0.47 ± 0.04			experiment[b]
		Present Results				
0.63	0.07	0.14	0.17	0.13	0.04	total
0.48	0.06	0.07	0.40	0.37	0.03	direct
0.68	0.07	0.16	0.09	0.04	0.05	indirect
		Results from Ref 1				
0.53	0.08	0.10	0.29	0.25	0.04	total[c]
0.48	0.07	0.07	0.37	0.33	0.04	direct[c]
0.66	0.09	0.16	0.08	0.04	0.04	indirect[c]

[a] The contributions from the *direct* and *indirect* mechanisms are also indicated. [b] Reference 12. [c] Calculations on the B3LYP/cc-pVTZ PES of ref 1.

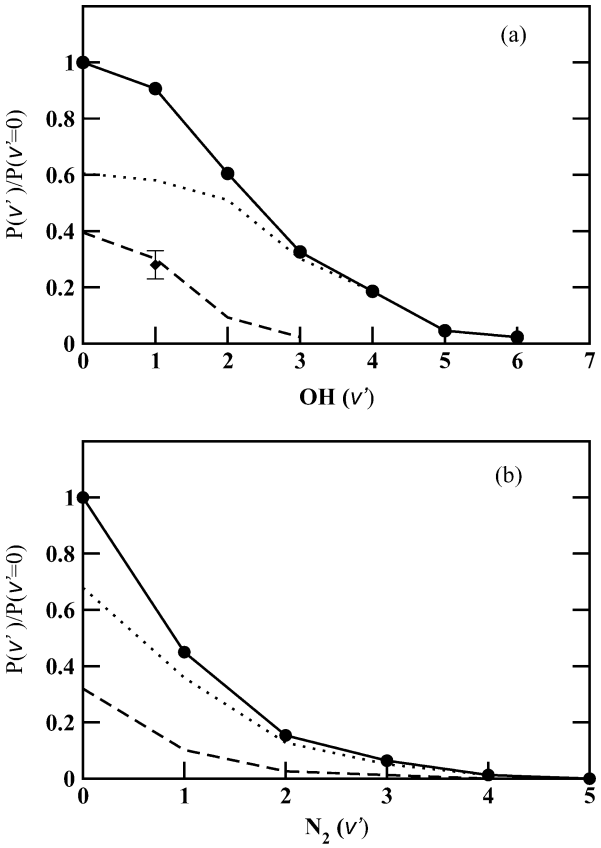

Figure 4. (a) OH vibrational branching ratios relative to $v' = 0$ at E_t = 1.48 eV. Solid circles, present QCT results. Solid diamond with error bar: experimental result from ref 12. (b) Present N_2 vibrational branching ratios relative to $v' = 0$ calculated at E_t = 1.48 eV. The contributions from the *direct* and *indirect* mechanisms are depicted with dashed and dotted lines, respectively.

Table 8 shows the comparison between the present QCT and the experimentally deduced[12] energy disposal data at E_t = 1.48 eV. The main difference between theory and experiment is found

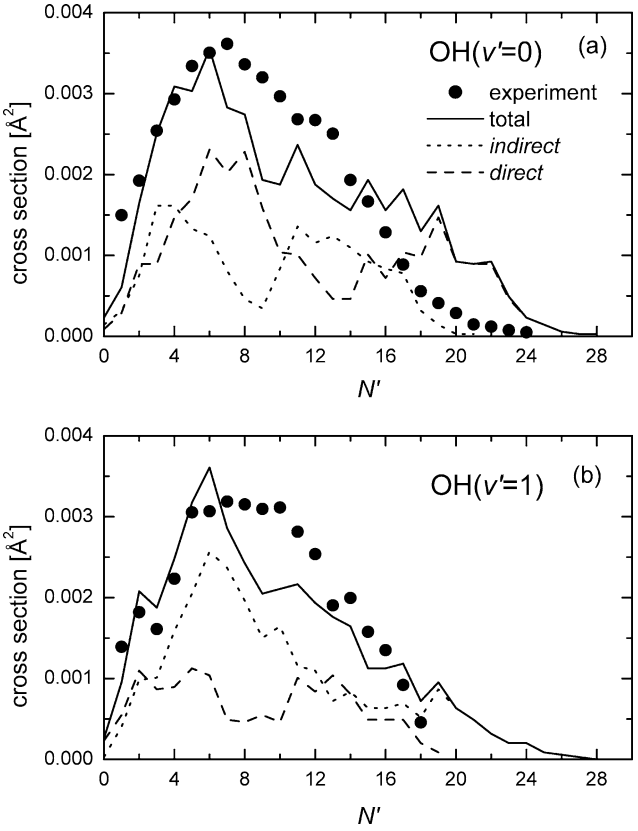

Figure 5. Rotational distributions at $E_t = 1.48$ eV. Solid line, present QCT results. Solid circles, experimental results from ref 12. Dotted line, contribution from the *indirect* trajectories. Dashed line, contribution from the *direct* trajectories. (a) OH($v' = 0$) and (b) OH($v' = 1$).

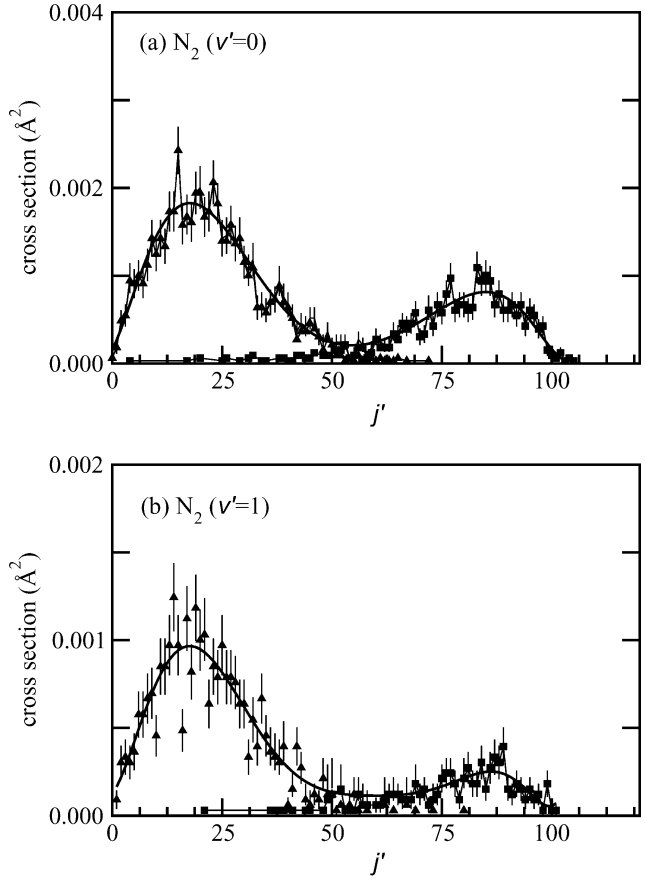

Figure 6. (a) Solid line, QCT rotational distribution for $N_2(v' = 0)$ products at $E_t = 1.48$ eV. The solid line is an eighth-degree polinomial fit to the QCT distribution. Solid triangles with error bars, contribution from the *indirect* trajectories. Solid squares with error bars, contribution from the *direct* trajectories. (b) QCT rotational distribution for $N_2(v' = 1)$ products at $E_t = 1.48$ eV.

in the internal excitation of N_2 (17 vs 47% of the total energy available). The present QCT calculations show that the *direct* mechanism is responsible for most of the rotational excitation of the N_2 molecule (37%), whereas the *indirect* mechanism accounts for very little rotational excitation of N_2 (9%). In the previous QCT study on the B3LYP/cc-pVTZ PES,[1] almost the same energy partitioning for both *direct* and *indirect* mechanisms was obtained (see Table 8), but given that the direct mechanism is predominant in that PES, the internal energy content of the N_2 molecule was higher than in the present case.

As it was pointed out in our previous work,[1] the large amount of N_2 rotational excitation produced in the reaction through the *direct* mechanism is somewhat unexpected, since the NNO angle in the present H−ONN transition state is 160°, and it seems unlikely that a torque on the departing N_2 can be produced. However, while the NNO angle changes significantly along the reaction coordinate containing the H−ONN transition state (160−130°), this same angle along the MEP that contains the [NNOH] transition state only varies slightly (from 95° to 105°). Thus, it seems that strong repulsive forces participate along the pathway involving the H−ONN transition state, exerting a significant torque on the N_2 molecule. This explanation is consistent with the fact that the rotational excitation of the N_2 produced by the direct mechanism is largely independent of collision energy. Momentum transfer from the incoming H atom is very inefficient as a mechanism for rotational excitation in this reaction.

B. Product Population Distributions and OH State-Specific Energy Disposal. Figure 4 depicts the QCT OH and N_2 vibrational branching ratios relative to $v' = 0$, $P(v')/P(v' = 0)$, calculated at 1.48 -eV collision energy. In both cases, the most populated vibrational state is $v' = 0$. The contributions from the *direct* and *indirect* trajectories are also portrayed in Figure 4. As can be seen, for the OH product the minor *direct* mechanism does not show any population inversion, whereas for the reaction through the major *indirect* mechanism the population of $v' = 0$ is nearly equal to that of $v' = 1$. The $P(v' = 1)/P(v' = 0)$ ratio for the OH product determined experimentally by Brouard et al.[12] at this collision energy is 0.28 ± 0.05, which differs considerably from that obtained in the present calculations. Wittig and co-workers[5] obtained an experimental value of 0.5, which is also far from the present result of 0.95. Clearly, this result seems to be at variance with both experimental values even if we consider the apparent discrepancy between them. The $P(v' = 1)/P(v' = 0)$ ratio obtained for direct trajectories matches the experimental value by Brouard et al., but given the preponderance of the indirect mechanism, this agreement can only be considered fortuitous. Similar behavior was found in the previous study using a B3LYP PES. In that case, however, since the contribution of direct trajectories was larger, the branching ratio was in better agreement with the experimental result.

Figure 5 shows the comparison between the present QCT rotational distributions for OH($v' = 0$) and OH($v' = 1$) and those experimentally determined in the experiments of Brouard and co-workers at $E_t = 1.48$ eV. In this comparison, the OH total angular momentum apart from electron spin, N', has been equated to j', the rotational angular momentum employed in the QCT calculations, where the OH molecule is treated as a closed-shell species. This is a good approximation for high enough N' levels ($N' \geq 5$) in terms of rotational energy.[32] There

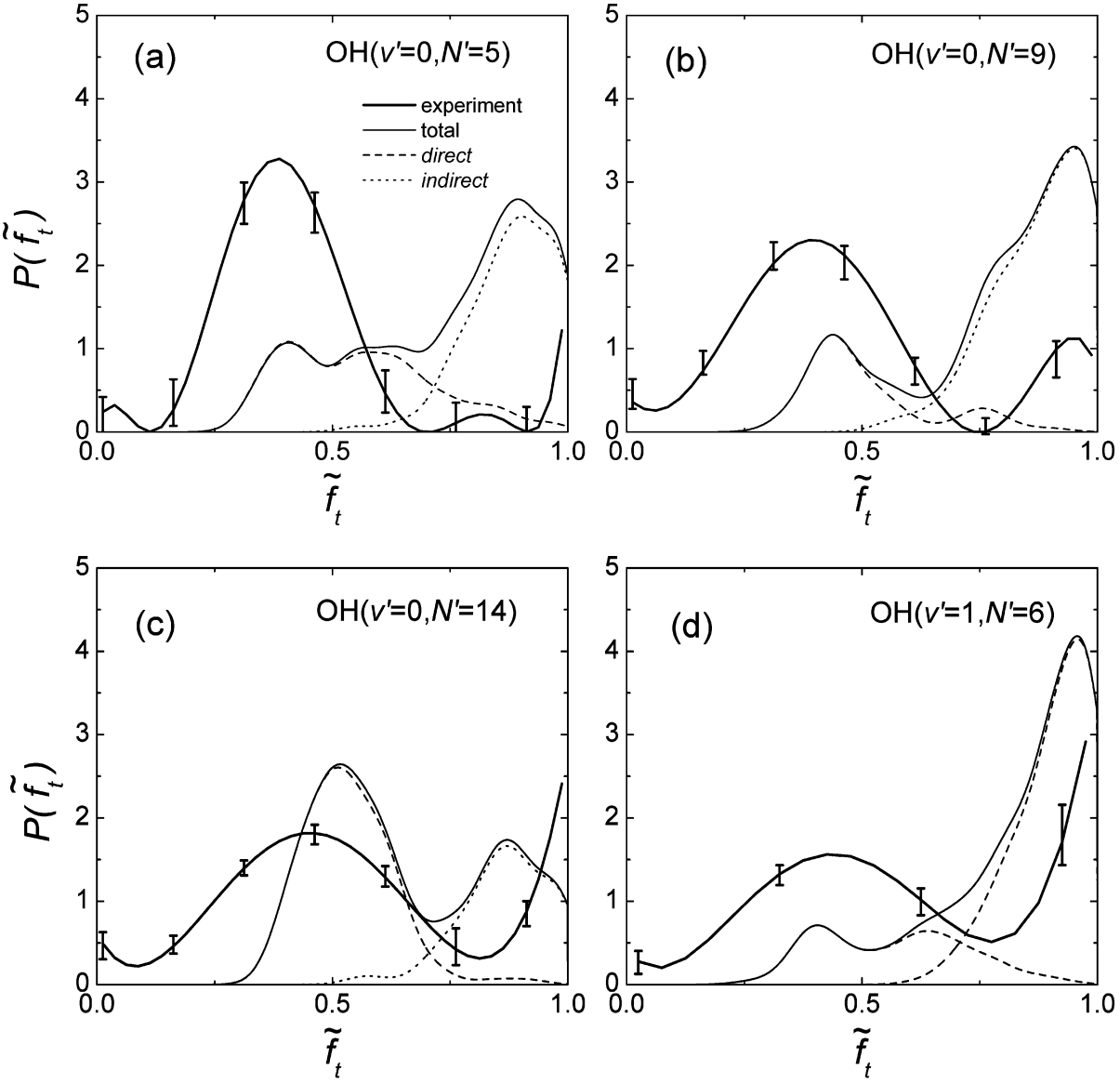

Figure 7. Distributions of the fraction of the available energy appearing as product translation, $P(\tilde{f}_t)$, for selected OH rovibrational states. (a) Solid line, QCT results for OH($v' = 0$, $N' = 5$). Dotted line, contribution from the *direct* trajectories. Dot−dashed line, contribution from the *indirect* trajectories. Solid thick line with error bars, experimental results for OH($^2\Pi_{3/2}$; A″, $v' = 0$, $N' = 5$) from ref 12. (b, c, and d) Same as part a but for OH($v' = 0$, $N' = 9$), OH($v' = 0$, $N' = 14$), and OH($v' = 1$, $N' = 6$), respectively.

is a reasonable agreement between theory and experiment, although the QCT distribution for OH($v' = 0$) is somewhat hotter than the experimental one. The theoretical distributions have been analyzed in terms of direct and indirect trajectories, and the results are also shown in Figure 5. Interestingly, both *direct* and *indirect* OH($v' = 0$) rotational distributions show a clear bimodality with shifted maxima. Whereas the rotational distribution corresponding to the indirect trajectories peaks at $N' = 3$ and $N' = 11-12$, showing a minimum at $N' = 8-9$, that arising from the direct trajectories peaks at $N' = 6-8$ and $N' = 18-20$, with a minimum at $N' = 13-14$. Thus, it seems to be a correlation between the maxima and minima of the *direct* and *indirect* OH($v' = 0$) rotational distributions. Analysis of individual trajectories indicates that for the direct trajectories, small-impact parameters *b* contribute almost exclusively to low rotational states ($N' \leq 10$), whereas large *b* values contribute to high N' states. This correlation is not so clear, however, for the indirect trajectories. Similar bimodality was observed in our previous QCT study for the title reaction on the B3LYP/cc-pVTZ PES (see Figure 4 in ref 1). For the OH($v' = 1$) channel, the bimodality is not so clear although there is some reminiscence of it.

The corresponding QCT $N_2(v' = 0)$ and $N_2(v' = 1)$ rotational distributions calculated at 1.48-eV collision energy are depicted in Figure 6. In this case, there are no direct measurements of N_2 rotational populations to compare with. The rotational distributions are clearly bimodal, peaking around $j' = 15$ and ′80. As can be seen, *indirect* trajectories lead to low rotational states of N_2, while *direct* trajectories yield N_2 in high rotational states. This result agrees with that obtained previously on the B3LYP/cc-pVTZ PES,[1] but in the present case, the indirect trajectories (low rotational excitation) are predominant over the direct trajectories (high rotational excitation), just the opposite of that in the calculations on the B3LYP/cc-pVTZ PES.

Brouard and co-workers[11,12] derived the kinetic energy release distributions for specific v', N' states of the OH product molecule from the analysis of the Doppler profiles. From these distributions, information about the internal energy of the N_2 coproduct was inferred. We have calculated the corresponding QCT $P(\tilde{f}_t)$ for specific state-resolved OH(v', N') as described in section

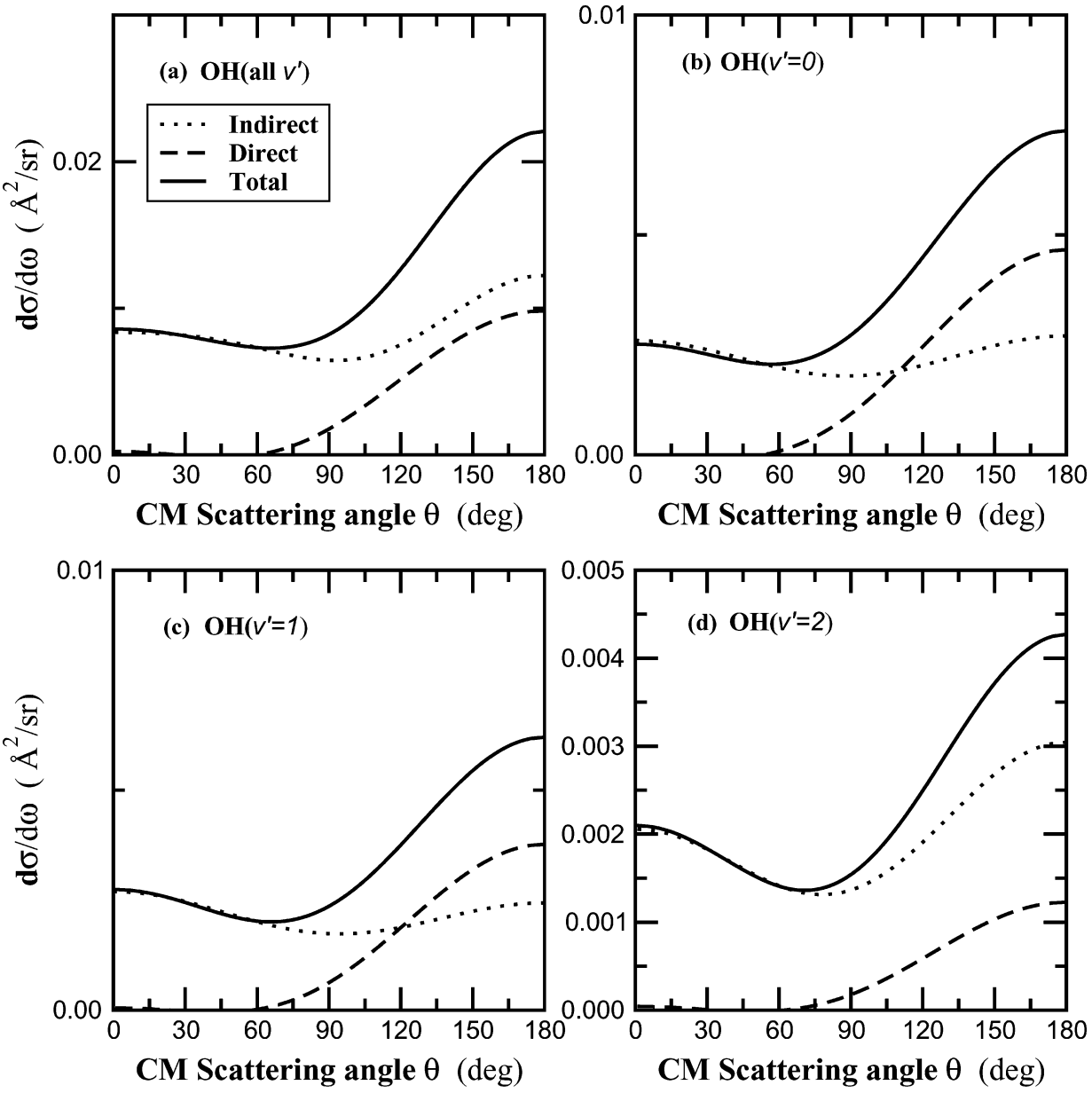

Figure 8. Total (a) and vibrationally state-resolved (b, c, d) differential cross sections calculated for the title reaction at $E_t = 1.48$ eV. The contributions from the *direct* (dashed line) and *indirect* (dotted line) trajectories are also depicted.

III. The comparison between experiment and theory is shown in Figure 7 for different v', N' states of OH. The contributions from the direct and indirect trajectories are also included in the figure. The QCT $P(\tilde{f}_t)$ values are clearly bimodal and reproduce the experimentally derived only qualitatively. As can be seen, the peak at $\tilde{f}_t \leq 0.5$ in the QCT distributions is due uniquely to *direct* trajectories, whereas the high $\tilde{f}_t$ component is mainly accounted for by the *indirect* trajectories. The corresponding $P(\tilde{f}_t)$ values calculated on the B3LYP/cc-pVTZ PES[1] had also two components, but in that case, the contribution of direct trajectories was noticeably larger than that from indirect trajectories, and thus the $P(\tilde{f}_t)$ values peaked at $\tilde{f}_t \leq 0.5$. As discussed in ref 1, Brouard et al. compared the OH($v' = 0$, $N' = 5$) $P(f_t)$ for the H + N_2O reaction with that obtained in the photodissociation of N_2O from the first absorption band[37] and observed an excellent agreement. They concluded that the product N_2 molecules are generated in high rotational states. The present and previous[1] QCT calculations support the conclusion that the N_2 product must appear rotationally excited rather than vibrationally excited. The present study provides additional support for the existence of two mechanisms, but it differs from the interpretation of Brouard and co-workers in that the *direct* mechanism is the one yielding rotationally hot N_2, whereas translationally excited N_2 molecules are produced by the *indirect* mechanism.

C. Differential Cross Sections. The QCT total and OH vibrationally state-resolved (summed on all N_2 final states) DCSs calculated for the title reaction at 1.48-eV collision energy are depicted in Figure 8, along with the contributions from the *direct* and *indirect* trajectories. As can be seen, the total DCS is predominantly backward with a large contribution in the sideways and forward regions. Direct trajectories yield a purely backward DCS, whereas the DCS corresponding to the indirect trajectories is nearly forward−backward symmetric. This makes sense considering the two prototypic mechanisms involved in the title reaction: direct trajectories correspond to a purely abstraction mechanism, characterized by scattering in the backward hemisphere, whereas a complex mechanism is related with the indirect trajectories yielding a practically isotropic DCS.

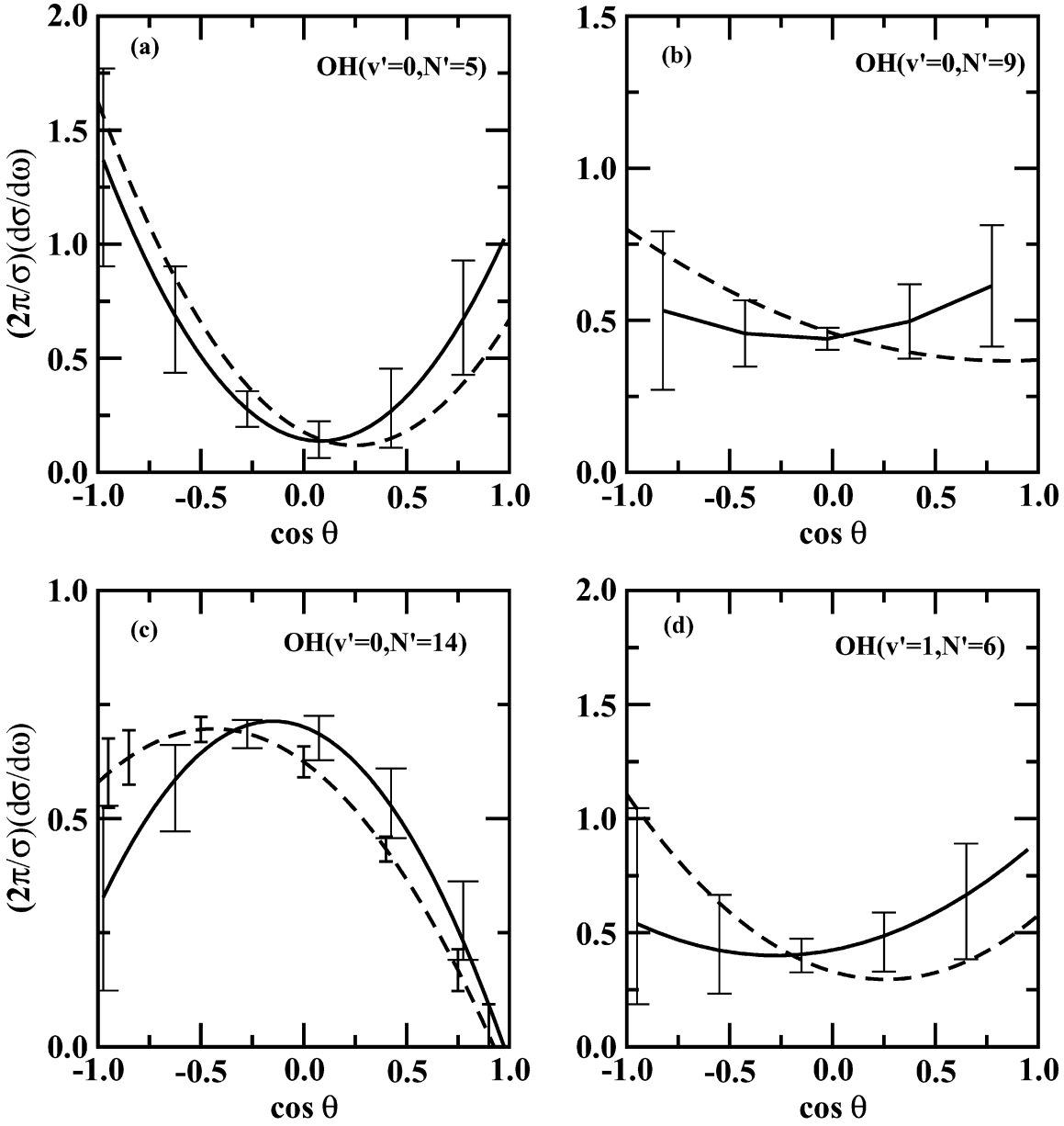

Figure 9. Comparison between experimental and QCT OH(v', N') state-resolved DCSs for the H + N_2O reaction at $E_t = 1.48$ eV. Solid lines with error bars: experimental DCSs from ref 12. Dashed lines: present QCT calculations.

Similar conclusions can be obtained for the OH v' state-resolved DCSs also shown in Figure 8.

Fully OH(v', N') state-resolved DCSs calculated at $E_t = 1.48$ eV are depicted in Figure 9 and compared with those experimentally deduced by Brouard et al.[12] The QCT DCSs are normalized by the factor $2\pi/\sigma$ and represented against cos θ. The agreement found between theory and experiment is quite remarkable. The experimental DCSs show a trend of shifting from forward−backward symmetry at low N' to more sideways at high N'. The QCT DCSs have a similar behavior although the angular distributions are somehow more backward peaking than the experimental DCSs. In contrast, the DCSs calculated on the B3LYP/cc-pVTZ PES[1] were clearly at variance with the experimental determinations and, thus, with the present calculations on the more sophisticated QCISD PES.

The overall angular-recoil velocity information can be summarized in the triple DCSs for specific v', N' states of OH, shown as scattering angle-recoil velocity of OH polar maps and 3D perspectives in Figures 10 and 11. The information that can be obtained from these polar maps corresponds to the N_2 cofragment produced in coincidence with the different v', N' states of OH. It should be stressed that the calculated polar maps clearly show that angular and velocity distributions are coupled. The bimodality of the final state distribution of N_2 commented on above (see Figures 6 and 7) is also clearly observed in the present polar maps. The outer ring, which is nearly isotropic, corresponds to the indirect trajectories, while the direct trajectories give rise to the inner ring in the plots, being predominantly backward and sideways. The resulting angle-velocity DCS depends considerably on the OH quantum state that is sampled. As the final OH($v' = 0$) rotational state increases from $N' = 5$ to ′14, the angular distribution associated with the direct mechanism shifts progressively from backward scattering to sideways. Moreover, the relative contribution of the two mechanisms is clearly seen in the plots and follows the tendency observed in the rotational distributions of the OH product (see upper panel of Figure 5). The plot corresponding to OH($v' = 0$, $N' = 6$) is in fairly good agreement with the nonseparable polar map experimentally deduced by Brouard and co-workers (Figure 12 of ref 12).

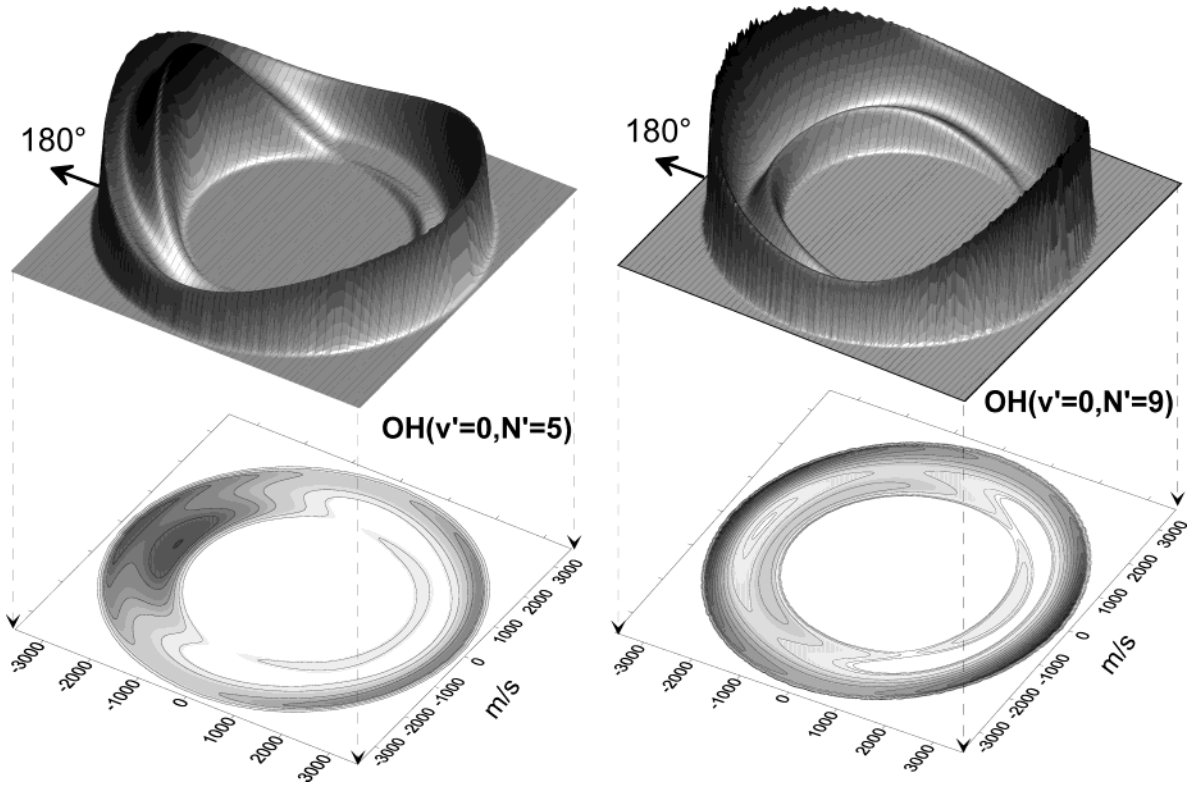

Figure 10. Scattering angle-recoil velocity polar maps and 3D perspectives of the triple differential cross-sections for the title reaction at $E_t = 1.48$ eV yielding OH($v' = 0$, $N' = 5$) and OH($v' = 0$, $N' = 9$) product molecules. The information contained in these plots corresponds to the N_2 cofragment produced in coincidence with the different v', N' states of OH.

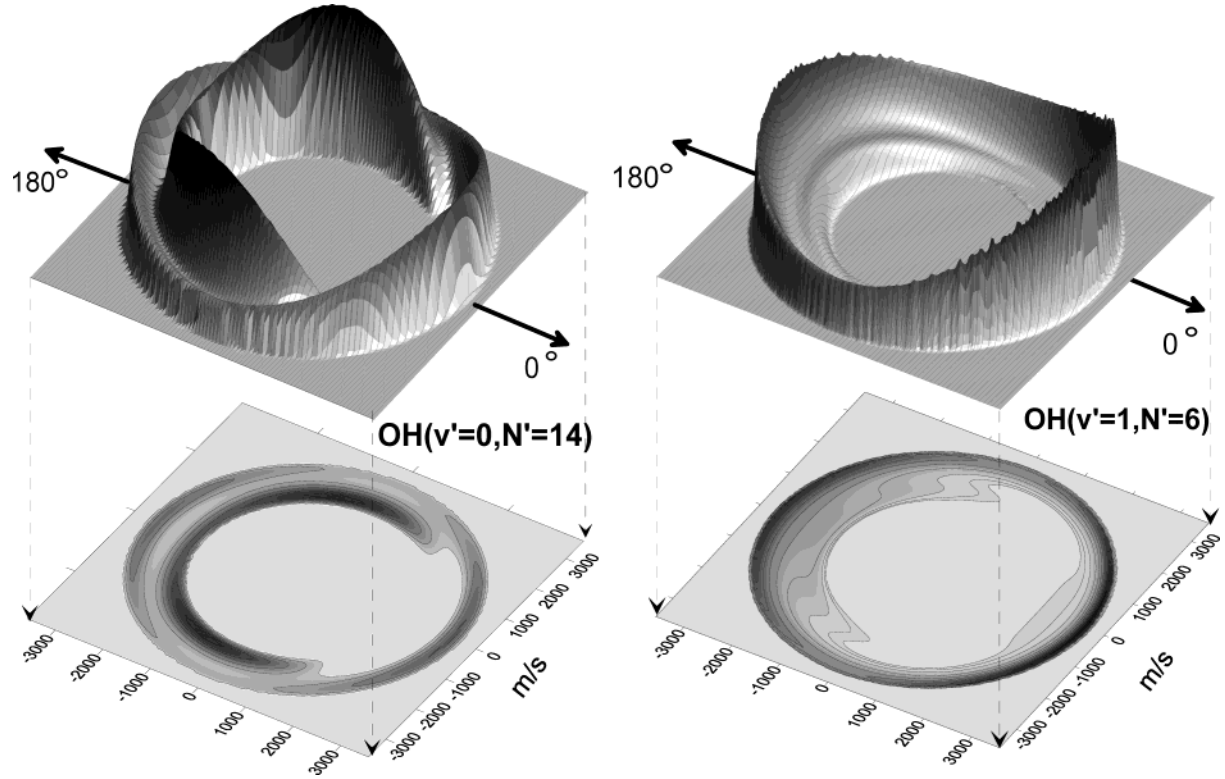

Figure 11. Same as in Figure 10 but for OH($v' = 0$, $N' = 14$) and OH($v' = 1$, $N' = 6$).

V. Conclusions

The dynamics of the H + $N_2O \rightarrow$ OH + N_2 reaction has been studied by means of quasiclassical trajectory calculations on a new ab initio PES calculated at the QCISD/cc-pVDZ and cc-pVTZ levels of theory using the iterative and interpolation methods implemented in the GROW package by Collins and co-workers. The final PES has been refined by calculating all the energies of the ab initio points at the QCISD(T)/cc-pVTZ level of theory.

The dynamics of the title reaction is determined by two different mechanisms, which are classified as *direct* or *indirect* according to whether the H atom attacks the O side or the N

side of the N_2O molecule. Analysis of collision times supports the existence of these two mechanisms. The indirect mechanism is found to be the preferred one for the reaction at low collision energies. As translation energy increases, the fraction of trajectories that follow the *direct* mechanism increases up to 30%.

The calculated total reaction cross sections vs collision energy are found in good agreement with the recently measured absolute values at collision energies lower than 1.20 eV. At higher collision energies, the QCT integral cross sections are well below those experimentally determined. Although there is a serious discrepancy in the predicted $v' = 1/v' = 0$ vibrational branching ratio with respect to that obtained experimentally, the OH rotational populations at the collision energy $E_t = 1.48$ eV reproduce most of the features of the experimental data.

The predicted N_2 vibrational distribution is *cold*, while the rotational distribution is quite *hot*, confirming previous interpretations with respect to the nature of the observed internal excitation of N_2. It is also demonstrated that the indirect trajectories yield translationally hot and rovibrationally cold N_2 molecules, confirming the bimodality of the recoil energy distributions found experimentally. However, the agreement between the calculated and experimentally derived kinetic energy release distributions for specific OH rovibrational states is only qualitative.

The QCT calculations on the present ab initio PES yield results that reproduce quite well all the available experimental measurements of the OH state-resolved differential cross sections. In particular, the theoretical calculations indicate that the direct trajectories give rise to predominantly backward-sideways scattering, while the products formed by the indirect mechanism are isotropically scattered. It is also found that there exists a strong pair-correlation between the OH and N_2 products formed in coincidence; that is, for one of the coproducts, the overall angular and velocity distribution largely depends on the particular rovibrational state of the other product.

Overall, the present results seem to be in better agreement with the existing body of experimental results and some crucial aspects of the topology of the PES have been clarified. However, some important discrepancies with the experimental data still remain. To further improve the agreement with the experimental results, a higher level of ab initio calculations for the PES and/or the concurrence of quantum mechanical scattering calculations may possibly be required.

Acknowledgment. We thank Mark Brouard and Rick Fletcher for communicating their experimental results and for valuable discussions. J.F.C. acknowledges support from the Spanish Ministry of Science and Technology through the program "Ramón y Cajal", the "Fundación Flores-Valles-UCM" for a visiting fellowship to the Research School of Chemistry (RSC) (Australian National University, Canberra, Australia), and the RSC for additional contribution to the visiting fellowship. The Spanish part of this work has been financed by DGES of Spain (Project BQU2002-04627-C02-02) and by the European Commission within the RT Network *Reaction Dynamics* (Contract No. HPRN-CT-1999-00007).

References and Notes

(1) Castillo, J. F.; Collins, M. A.; Aoiz, F. J.; Bañares, L. *J. Chem. Phys.* **2003**, *118*, 7303.

(2) Hollinsworth, W. E.; Subbiah, J.; Flynn, G. W.; Weston, R. E. *J. Chem. Phys.* **1985**, *82*, 2295.

(3) Hoffmann, G.; Oh, D.; Iams, H.; Wittig, C. *Chem. Phys. Lett.* **1989**, *155*, 356.

(4) Hoffmann, G.; Oh, D.; Wittig, C. *J. Chem. Soc., Faraday Trans. 2* **1989**, *85*, 1141.

(5) Böhmer, E.; Shin, S. K.; Chen, Y.; Wittig, C. *J. Chem. Phys.* **1992**, *97*, 2536.

(6) Marshall, P.; Fontijn, A.; Melius, C. F. *J. Chem. Phys.* **1987**, *86*, 5540.

(7) Walch, S. P. *J. Chem. Phys.* **1993**, *98*, 1170.

(8) Bradley, K. S.; McCabe, P.; Schatz, G. C.; Walch, S. P. *J. Chem. Phys.* **1995**, *102*, 6696.

(9) Bradley, K. S.; Schatz, G. C. *J. Phys. Chem.* **1996**, *100*, 12154.

(10) Fletcher, T. R.; Wocjick, M. D. *Phys. Chem. Earth.* **2001**, *26*, 487.

(11) Brouard, M.; Burak, I.; Gatenby, S. D.; Markillie, G. A. J. *Chem. Phys. Lett.* **1998**, *287*, 682.

(12) Brouard, M.; Burak, I.; Gatenby, S. D.; Hart, D.; Minayev, D. *J. Chem. Phys.* **1999**, *110*, 11335.

(13) Brouard, M.; Burak, I.; Gatenby, S. D. *Phys. Chem. Chem. Phys.* **2000**, *2*, 715.

(14) Brouard, M.; Gatenby, S. D.; Joseph, D. M.; Vallance, C. *J. Chem. Phys.* **2000**, *113*, 3162.

(15) Jordan, M. J. T.; Thompson, K. C.; Collins, M. A. *J. Chem. Phys.* **1995**, *102*, 5647.

(16) Thompson, K. C.; Jordan, M. J. T.; Collins, M. A. *J. Chem. Phys.* **1998**, *108*, 8302.

(17) Bettens, R. P. A.; Collins, M. A. *J. Chem. Phys.* **1999**, *111*, 816.

(18) Zhang, D. H.; Collins, M. A.; Lee, S.-Y. *Science* **2000**, *290*, 961.

(19) Yang, M.; Zhang, D. H.; Collins, M. A.; Lee, S.-Y. *J. Chem. Phys.* **2001**, *115*, 174.

(20) Becke, A. D. *J. Chem. Phys.* **1993**, *98*, 5648.

(21) Chuang, Y.-Y.; Coutino, E. L.; Truhlar, D. G. *J. Phys. Chem. A* **2000**, *104*, 446.

(22) Frisch, M. J.; Trucks, G. W.; Schlegel, H. B.; Scuseria, G. E.; Robb, M. A.; Cheeseman, J. R.; Zakrzewski, V. G.; Montgomery, J. A., Jr.; Stratmann, R. E.; Burant, J. C.; Dapprich, S.; Millam, J. M.; Daniels, A. D.; Kudin, K. N.; Strain, M. C.; Farkas, O.; Tomasi, J.; Barone, V.; Cossi, M.; Cammi, R.; Mennucci, B.; Pomelli, C.; Adamo, C.; Clifford, S.; Ochterski, J.; Petersson, G. A.; Ayala, P. Y.; Cui, Q.; Morokuma, K.; Malick, D. K.; Rabuck, A. D.; Raghavachari, K.; Foresman, J. B.; Cioslowski, J.; Ortiz, J. V.; Stefanov, B. B.; Liu, G.; Liashenko, A.; Piskorz, P.; Komaromi, I.; Gomperts, R.; Martin, R. L.; Fox, D. J.; Keith, T.; Al-Laham, M. A.; Peng, C. Y.; Nanayakkara, A.; Gonzalez, C.; Challacombe, M.; Gill, P. M. W.; Johnson, B. G.; Chen, W.; Wong, M. W.; Andres, J. L.; Head-Gordon, M.; Replogle, E. S.; Pople, J. A. *Gaussian 98*, revision A.9; Gaussian, Inc.: Pittsburgh, PA, 1998.

(23) Kendall, R. A.; Dunning, T. H., Jr.; Harrison, R. J. *J. Chem. Phys.* **1992**, *96*, 6796.

(24) Patel-Misra, D.; Dagdigian, P. J. *J. Phys. Chem.* **1992**, *96*, 3232.

(25) Haworth, N. L.; Mackie, J. C.; Bacsay, G. B. *J. Phys. Chem. A* **2003**, *107*, 6792.

(26) Laursen, S. L.; Delia, A. E.; Mitchell, K. *J. Phys. Chem.* **2000**, *104*, 3681.

(27) Thompson, K. C.; Collins, M. A. *J. Chem. Soc., Faraday Trans.* **1997**, *93*, 871.

(28) Ischtwan, J.; Collins, M. A. *J. Chem. Phys.* **1994**, *100*, 8080.

(29) Jordan, M. J.; Thompson, K. C.; Collins, M. A. *J. Chem. Phys.* **1995**, *102*, 9669.

(30) Castillo, J. F.; Santamaría, J. *J. Phys. Chem. A* **2000**, *104*, 10414.

(31) Castillo, J. F.; Aoiz, F. J.; Bañares, L.; Santamaría, J. *Chem. Phys. Lett.* **2000**, *329*, 517.

(32) Castillo, J. F.; Aoiz, F. J.; Bañares, L. *Chem. Phys. Lett.* **2002**, *356*, 102.

(33) Hase, W. L., et al. *QCPE*, **1996**, *16*, 671.

(34) Martínez, M. T.; Hernandez, M. L.; Alvariño, J. M.; Aoiz, F. J.; Sáez Rábanos, V. *J. Chem. Phys.* **2003**, *119*, 7871.

(35) Bañares, L.; Aoiz, F. J.; Honvault, P.; Launay, J.-M. *J. Phys. Chem. A* **2004**, *108*, 1616.

(36) Brouard, M.; Burak, I.; Marinakis, S.; Minayev, D.; OKeeffe, P.; Vallance, C.; Aoiz, F. J.; Bañares, L.; Castillo, J. F.; Zhang, D. H.; Xie, D.; Yang, M.; Lee, S.-Y.; Collins, M. A. *Phys. Rev. Lett.* **2003**, *90*, 093201.

(37) Hanisco, T. F.; Kummel, A. C. *J. Phys. Chem.* **1993**, *97*, 7242.